Electronic structure of α-alumina and its defect states

S. Ciraci*

*Institut für Grenzflächenforschung und Vakuumphysik, Kernforschungsanlage Jülich, Postfach 1913,
D-5170 Jülich, West Germany*

Inder P. Batra

IBM Research Laboratory, San Jose, California 95193

We have investigated the electronic structure of α-alumina and its defect states by using a semiempirical method. Our results show that the fundamental gap is indirect, and the charge transfer enhances the hybridization of aluminum and oxygen orbitals, which in turn leads to the broad upper and lower valence bands. Using the calculated total and orbital density of states, we have provided a consistent interpretation of the existing spectra. For the ideal α-Al_2O_3(0001) surface we have found that the Al—O bonds at the surface have a considerable covalent character and the Al—dangling bonds produce the major surface-state band. Energy positions of the oxygen-vacancy states, and of the surface states, strongly suggest that the oxygen deficiency is responsible for some of the low-energy structures in the excitation spectra.

I. INTRODUCTION

There are several reasons that have motivated us to carry out such a study as this. First of all, Al_2O_3 is one of the main constituents of minerals, and thus its electronic structure is of great interest to mineralogists. Technologically, the Al_2O_3 crystal (alumina) is known to be an insulator with a large band gap, and is able to remain transparent even after exposures to high doses of radiation. These properties, together with its chemical inertia, have made alumina a material of frequent use in technological applications. Academically, the physical properties of oxides,[1-3] especially those of SiO_2, have attracted great interest because of a widespread application of metal-oxide-semiconductor (MOS) transistors. A number of investigations have recently revealed information concerning the electronic structure and the bonding of SiO_2. As for Al_2O_3, our understanding regarding the bands and bonds is far from complete. Attempts in this direction have, in the past, concentrated on the spectral measurements. One was able to deduce broad features of the electronic structure from the results of several optical-absorption spectroscopies,[4-8] as well as x-ray emission spectroscopy[4,8-10] (XES), x-ray photoemission spectroscopy[11,12] (XPS), and electron-energy-loss[13] (EELS) spectroscopy. Yet there is no theoretical work providing a consistent interpretation of the spectra. It is now well accepted that the valence states are grouped into two bands, but there appears to be no consensus on the widths of these bands, and on the value of the fundamental band gap as well. The low-energy structures in the excitation spectra have prevented an unambiguous determination of the fundamental band gap. Although these structures have commonly been attributed to the exciton absorption,[6,11,13] the downward shift observed in amorphous Al_2O_3 may possibly be due to the contribution of defect states.[11] Investigations on a similar oxide, namely SiO_2, indicated that the defect states do in fact play an important role in the applications of electronic devices.[14,15] The surfaces of α-Al_2O_3 (corundum), apart from their possible connections with the gap states,

display interesting properties.[16-18] Low-energy electron diffraction (LEED) studies revealed that the α-Al_2O_3(0001) surface is bulklike and stable up to $\sim 1250\,°C$. Above this temperature the ordered surface reconstructs into a rotated $(\sqrt{31} \times \sqrt{31})$ structure, with simultaneous evaluation of oxygen. The aluminum atoms of the high-temperature surface phase are found to exhibit a reduced oxidation state.[18]

The study of alumina is also important because Al_2O_3 can be considered as the final stage in the oxidation of the Al surfaces. In that respect a complete understanding of Al_2O_3 crystals is expected to give more insight into the underlying physics of the intermediate oxidation stage.[19] As a matter of fact, recent studies have clearly established that as soon as oxygen resides between the two topmost layers of the Al surface its immediate vicinity becomes oxidelike.[20-22]

Despite all the experimental data accumulated so far, most theoretical electronic structure calculations have been semiquantitative[23,24] or molecular,[25,26] in nature. Evarestov *et al.*[27] calculated the energy-band structure of α-alumina by using the semiempirical Mulliken-Rudenberg technique. Recently, Batra[28] reported a realistic band structure by the extended tight-binding method. In his work the emphasis was placed on the bonding, but no detailed account of the experimental spectra was given. In the present work we have investigated the electronic structure of Al_2O_3 crystals, and of some defect states. Even though Al_2O_3 is found in different structural forms (such as α-, γ-, and a-Al_2O_3), spectral data indicate that broad features of their state densities are similar.[4,11] We therefore have taken α-alumina as a prototype in our study. As discussed extensively in Sec. II, calculations have been performed by using a semiempirical method which allows the incorporation of the charge transfer between Al and O. In Sec. III, the energy bands and state densities are presented with an emphasis on the analysis of states in terms of the atomic orbitals. Results show that α-alumina has valence states grouped in two broad bands, and an indirect band gap, and also differs from the well-

known oxide of Si in some respects. In order to deduce a structural unit, which describes basic properties of alumina, the electronic structures of AlO_6 and Al_4O molecules have also been investigated. It is shown that the AlO_6 molecule can be taken as such a unit, though the band-structure effects are not negligible. A consistent interpretation of the existing spectra, and a brief discussion of the previous calculations, are also presented in the same section. Part of the purpose of this work is to shed light on the low-energy structures of the excitation spectrum and to learn more about the thin oxide films. In this context the electronic structure of the ideal α-Al_2O_3(0001) surface, and of the O and Al vacancies have, for the first time, been calculated. Results are outlined in Sec. IV. Evidence emerging from this study strongly suggests that the defect states should, at least partly, be responsible for the spectral structure in the band gap. Finally, the concluding remarks are given in Sec. V.

II. METHOD OF CALCULATIONS

Electronic structures have been calculated by a method that is derived from the extended Hückel theory (EHT).[29] It was shown that this method can be used to investigate the complicated structures, provided that the parameters are selected carefully. Several versions of this method have been proposed in the literature. Here, we use the form[30,31] which appears to work well for Al-O systems and has the following secular equation:

$$\sum_{j,n} \{[h_{ij}(\vec{R}_n) - E(\vec{k})]s_{ij}(\vec{R}_n, \vec{k})\}a_j(\vec{k}) = 0 \ . \tag{1}$$

$s_{ij}(\vec{R}_n, \vec{k})$ denotes the overlap integral between ith and jth Slater-type atomic orbitals[32,33] with an internuclear distance $\vec{R}_n$. It is weighted by a phase factor, $e^{i\vec{k}\cdot\vec{R}_n}$, and is properly normalized to yield $\sum_n s_{ii}(\vec{R}_n, \vec{k}) = 1$. An essential ingredient to the EHT calculations is the knowledge of the Hamiltonian matrix elements between various orbitals, which is obtained from the following empirical relation:

$$h_{ij}(\vec{R}_n) = K_{ij}(\vec{R}_n)(I_i I_j)^{1/2} \ . \tag{2}$$

In Eq. (2), K_{ij} is a parameter that is set equal to 1.0 for $R_n = 0$ and is usually taken as 2.5 for $\vec{R}_n \neq 0$. In the original theory the energy of the ith orbital I_i was assumed to be the negative of the corresponding ionization potential $I_{i,0}$. For a system with an appreciable amount of charge transfers the value of I_i is, however, expected to change.[30,31,34] In the first order this change can be formulated as

$$I_i = I_{i,0} - Q \Delta I_i \ . \tag{3}$$

In this equation Q is the effective charge of the atom (i.e., the orbital occupancy[35] minus the valency) and ΔI_i indicates the change of energy per unit charge transfer. In our study the essential idea has been to introduce $Q \Delta I_i$ and $K_{ij}(R \neq 0)$ as the parameters of the calculations, and to deduce their values from the experimental data. To achieve this, the basic premise used was that the charge is transferred from the metal ion to oxygen and that, as a consequence, the orbital energies of the cation and the anion vary in reverse directions. By changing the values

of parameters, one at a time, we have calculated the electronic structure of α-alumina. Figure 1 displays the major effects of each parameter on the calculated band structure. It is seen that decreasing value of the O $2p$ orbital energy causes the photoelectric threshold [i.e., the absolute energy of the valence-band maximum (VBM)] to decrease. Note that the atomic ionization potential (i.e., $I_i = I_{i,0}$) leads to a significantly large photoelectric threshold energy. Similarly, decreasing energy of the O $2s$ orbital raises the lower valence band (LVB) but has no significant effect on the other part of the band. Contrary to this, increased energy of the Al $3s$ orbital favors the hybridization with the oxygen orbitals. As a result, both the LVB and the upper valence band (UVB) become broader, and the intraband gap (between the UVB and the LVB) reduces. Furthermore, the fundamental energy gap becomes larger, in accordance with the trend observed in ionic semiconductors. The hybridization region of the valence band, as well as the energy of the lowest conduction band, are found to depend on the parameter K_{ij} ($i = $Al, $j = $O index).

It is clear that the interdependencies among various energy parameters, as seen in Eqs. (1) and (2), do not allow us to use a simple fitting procedure; we therefore obtain their values by the optimization of the calculated band structure with respect to the experimental data. In the optimization we incorporate the photoelectric threshold energy, the value of the fundamental band gap, and the broad features of the XPS spectrum, such as the widths of the UVB and the LVB, and the intraband gap—but not any specific structure—as the experimental input data. The reason for considering the photoelectric threshold is twofold. In the first place, the constant shift of all the orbital energies does not lead to a solid shift of the electronic structure obtained from Eq. (1). The photoelectric threshold enables us to determine the O $2p$ orbital energy unambiguously. Secondly, the electronic structures pertaining to the bulk alumina and to the defect states are presented on a unique energy scale. Owing to the charging effects
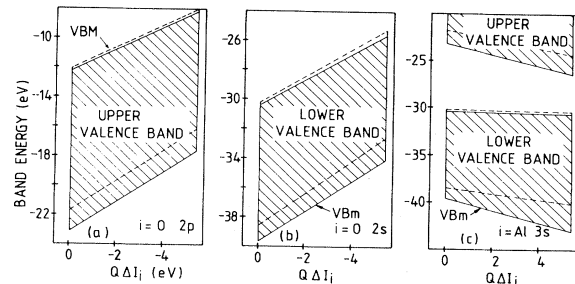

FIG. 1. Schematic description showing the influence of each orbital energy on the calculated energy band of α-alumina. (a) The UVB is raised and its width decreases as the energy of the O $2p$ orbital decreases. (b) The LVB is also raised with the decreasing energy of the O $2s$ orbital. (c) As the energy of the Al $3s$ orbital increases both the UVB and the LVB become broader and the intraband gap between them recedes. Bold and dashed lines indicate the band edges calculated for K_{ij} ($i = $Al, $j = $O)$= 2.5$ and $K_{ij} = 2.14$, respectively. $Q \Delta I_i$ denotes the change of the orbital energy with respect to the corresponding ionization potential. VBM and VBm denote the maximum and the minimum of the valence band, respectively.

no data is available regarding the binding energy of the VBM. Then, using the experimental data[21,36] we estimated the photoelectric threshold energy to be 9.0 ∓ 0.4 eV. The value of the fundamental gap is another set of experimental data that is important in the interpretation of the excitation spectrum. Uncertainties due to the exciton absorption in determining the fundamental gap have led to a range of values[6,11,13,28] (from 9.9 to 8.0 eV). In our calculations we have used the value of 8.5 eV deduced[13] from the intrinsic photoconductivity measurements,[37] which has certainly an important advantage over the other methods. Setting the experimental data this way, we have optimized the calculated band structure and have determined the parameters (i.e., $Q \, \Delta I_i$ and K_{ij}) therefrom. As for the overlap integrals, they are calculated analytically by converting the Slater-type valence orbitals[31] into the Gaussian-type orbitals. The overlaps of distant neighbors are taken into account until the preset convergence threshold ($\sim 10^{-7}$) is achieved.

In Table I we list the values of parameters and orbital data. At this point we would like to comment on the following points. First of all, due to the nature of the optimization process the calculated values may differ from the experimental data utilized in the optimization. Accordingly, the present method can be considered a scheme which uses the broad features of the spectrum to get insight on the detailed electronic structure. Moreover, by calculating orbital populations or by using the bond-order concept, new parameters that are proper for the defect states of the bulk solid can easily be generated. As a final remark, the method, as used in the present study, is similar in spirit to the empirical pseudopotential method.[38] In the latter, one fits the Fourier coefficients of the pseudo-potential to the spectral data, and obtains the energy eigenvalues and the pseudo-wave-functions by diagonalizing the secular equation. In the Slater-type orbitals[32,33] the shielding of core electrons was taken into account and the core orthogonalization part of the atomic orbitals is excluded. Therefore, our Bloch wave functions are comparable with the pseudo-wave-functions.

III. ELECTRONIC STRUCTURE OF α-Al$_2$O$_3$

A. Crystal structure

The atomic arrangement of α-alumina is characterized by that of chromium sesquioxide.[39] It has a rhombohedral symmetry (D_{3d}^6 space-group symmetry) and two Al$_2$O$_3$ units in the primitive cell. In this arrangement each Al atom is surrounded by six O atoms. Three of these oxygens lie at the corners of an equilateral triangle 2.58 a.u. above the central Al, and each forms an Al—O bond of 3.75 a.u. The remaining three form another equilateral triangle, which staggered with respect to the above one and which lies 1.51 a.u. below the central Al. Each O atom of the latter triangle is bound to Al by a stronger Al—O bond of 3.48 a.u. So a structural unit typified by AlO$_6$, which has an octohedral coordination, is constructed. In addition to this the valencies of cation and anion allow another combination, namely Al$_4$O, in which each O is surrounded by four Al, two each at 3.48 and 3.75 a.u. The z axis of the Cartesian coordinate system is taken

TABLE I. Normalized Gaussian-type atomic orbitals, energies of the orbitals, and other parameters used in the calculations.

	Orbital coefficients	Orbital exponent (a.u.$^{-1}$)	$I_{i,0}$ (eV)	$Q \, \Delta I_i$ (eV)	$K_{ij}(\vec{R}_n \neq 0)$
O 2s	−0.117 88	253.863 89	−32.244	−4.354	
	−0.183 75	40.660 87			
	−0.193 67	10.127 22			
	0.290 67	1.192 08			
	0.220 35	0.475 48			
	0.036 81	0.175 60			$K_{\text{O-O}} = 2.5$
O 2p	0.996 96	101.526 08	−15.782	−4.218	
	1.334 85	23.171 66			
	1.484 40	7.382 36			
	1.155 37	2.747 99			
	0.539 40	1.064 96			
	0.185 48	0.409 49			
	0.026 17	0.170 92			$K_{\text{Al-Al}} = 2.5$
Al 3s	−0.020 70	17.990 30	−11.292	5.422	
	−0.088 35	4.404 02			
	−0.161 14	1.519 87			
	0.208 69	0.291 51			
	0.062 55	0.143 63			$K_{\text{O-Al}} = 2.14$
Al 3p	−0.109 03	12.112 95	−5.986	4.081	
	−0.083 18	3.007 55			
	0.114 27	0.513 56			
	0.134 04	0.232 80			
	0.027 48	0.107 98			

along the vector $\vec{R}_1 + \vec{R}_2 + \vec{R}_3$ ($\vec{R}_i$ is the Bravais lattice vector). The symmetry properties of corundum structure are extensively discussed in Ref. 27. From the structure explained above one can also generate a hexamolecular cell, a larger cell containing 12 Al and 18 O atoms, that is referred to the hexagonal axes.[39] For the bulk α-alumina we use the rhombohedral symmetry, whereas the α-Al_2O_3(0001) surface is studied by the hexamolecular cell.

B. Energy-band structure and state densities

Figure 2(a) illustrates the energy-band structure along three axes of the rhombohedral Brillouin zone (BZ). The LVB extending from -36.4 eV up to -26.9 eV is 9.5 eV wide, and results mainly from the O2s orbitals. The lowest two bands are formed from the bonding combination of Al3s and O2s orbitals. The remaining four bands at about -27 eV have considerably small Al3p orbital contribution and are flat. A gap of 6 eV occurs between the LVB and the UVB. The UVB, in which O2p orbital contribution dominates, has a width of ~ 12 eV. In regard to the Al orbital contribution the UVB can tentatively be divided into three overlapping energy regions. Starting from the higher binding energies, states between -20.6 and ~ -16.0 eV exhibit a considerable Al3s orbital character. In going to lower binding energies, i.e., to the second region, Al3s contribution decreases, but Al3p contribution becomes significant. In these two regions, where Al and O orbitals hybridize, bands exhibit considerable dispersions, and bonds gain the covalent component. In the third region, between ~ -12 eV and the VBM, bands

are rather flat reflecting the nonbonding O2p orbital character as is common to many oxides. The VBM occurs at -8.8 eV along the Λ direction. In contrast to this, the conduction-band minimum (CBm) lies at Γ, and thus leads to an indirect band gap with a value of 8.7 eV. States at the bottom of the conduction band (CB) are generated from the antibonding combination of Al3s and O2s orbitals. As in Al metal, first the Al3s, and then the Al3p, orbital contributions become dominant as one goes upward in energy. For that reason the CB can be regarded as Al-like. This situation arises as a consequence of the high electronegativity of the O atom.[40]

In an effort to understand the basic aspects of the electronic structure and the importance of the band formation we next explore structural units[41] which may reproduce gross features of the spectrum. On the ground of localized Al—O bonds and in light of our discussion in Sec. III A, AlO_6 or Al_4O can be taken as such a fundamental unit. Indeed, $AlO_6{}^{9-}$ and Al_4O^{5-} oxyanions were, in the past, studied to extract information concerning the spectrum of the bulk oxide.[25] Using the bulk parameters, thereby simulating the crystalline environment, we have calculated the electronic structure of AlO_6 and Al_4O units and obtained the energy-level diagram shown in Figs. 2(b) and 2(c). To provide a comparison with the self-consistent field (SCF) cluster results,[25] closely lying levels (which are generated from the degenerate levels of perfect Al_6O) are averaged and labeled by the symmetry notation of the irreducible representation of the octahedral point group. The energy levels of AlO_6 display, in an obvious fashion, the LVB and UVB together with their three characteristic regions. The state $5a_{1g}$ is produced from the combination of Al3s and O2s orbitals, with a higher population on O atoms forming short Al—O bonds. The $6a_{1g}$ state has the Al3s orbital contribution, whereas the $5t_{1u}$ state displays a considerable Al3p component. Beyond the hybridization region, the closely lying states are pure O2p—like. Despite these resemblances, a comparison made between Figs. 2(a) and 2(b) demonstrates that molecular levels, especially those lying at the bottom of the bands, display considerable dispersions due to the interactions of neighboring Al—O bonds, emphasizing the importance of the band-structure effects. With regard to this point, further evidence can be obtained from the experimental data.[20] For example, O2p spectra of oxygen-covered Al(111) surfaces reveal that an increasing O exposure beyond 100 L (1 L = 1 langmuir = 10^{-6} Torr sec), wherein surface and subsurface oxygen coexist, is reflected in an increase of width at the Al-O hybridization region. As for the Al_4O unit, the states marked by $\times$ in Fig. 2(c) have an O orbital population over 20% and thus demonstrate the importance of the Al-Al interaction to get the actual width of the UVB. As is expected, the distribution is more Al-like and leads to states located in the gap.

Figure 3 presents the calculated total and orbital density of states.[40] The character of the bands necessitates a rather dense sampling in the BZ to obtain a finer structure, especially the high intensity originating from the flat bands. Nevertheless, state densities calculated by 16 and 64 $\vec{k}$ points were yielded resembling "gross" features. In panel (a) the state density of the UVB exhibits three broad peaks with finer structures superimposed. These peaks happen to coincide with the three characteristic regions.
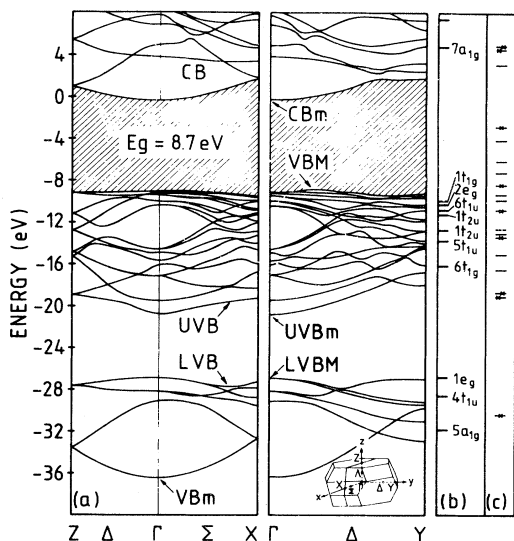

FIG. 2. (a) Energy-band structure of α-alumina calculated along three Cartesian axes: $X = (0.44487, 0.0, 0.0)$ a.u.$^{-1}$, $Y = (0.0, 0.70064, 0.0)$ a.u.$^{-1}$, and $Z = (0.0, 0.0, 0.38330)$ a.u.$^{-1}$. The inset shows the Brillouin zone. (b) Electronic energy-level diagram of the AlO_6 unit taken from the unit cell of α-alumina. (c) Same for Al_4O unit. States of Al_4O having more than 20% O orbital contribution are marked. Band energies in all figures are given with respect to the vacuum level explained in the text.
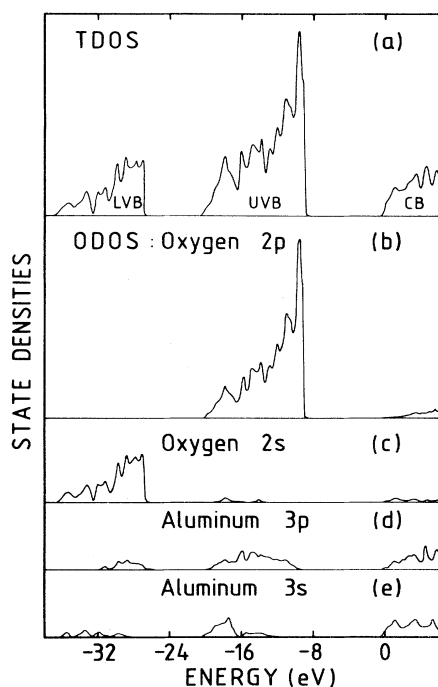
FIG. 3. State densities calculated by using 64 $\vec{k}$ points in the BZ and a broadening of 0.25-eV Gaussian half-width. (a) The total density of states (TDOS). (b), (c), (d), and (e) show the orbital density of states (ODOS) of various orbitals used in the calculations.

In the following panels, the total state density is projected on the basis orbitals of the constituent atoms. Despite the off-diagonal overlap terms in the population analysis, the distributions displayed in panels (b)—(e) are able to reasonably present the contribution of each orbital in various regions of the spectrum.

At this stage it is quite informative to compare the electronic structures of two well-known oxides, namely, silicondioxide and α-alumina[1,2,27,28,42−46]. In SiO_2 (in the form of α-quartz), a gap occurs in the UVB between the O $2p$ and the hybridization bands. In contrast to this, the hybridization bands of Al_2O_3 overlap with O $2p$ bands, probably due to the lower binding energies of Al orbitals. In spite of this, the width of the UVB is comparable in both oxides. Owing to the dispersions of the lowest bands, the LVB of Al_2O_3, however, depicts a higher width as compared to that of SiO_2. This unexpected situation will be discussed later, and can partly be attributed to the higher bond order in Al_2O_3. It is interesting to note that the band gaps of quartz and α-alumina are indirect.

C. Interpretation of the spectra

In providing a consistent interpretation the crucial point is the alignment of the calculated state density with respect to various experimental spectra; each depicts various states in the VB. Instead of shifting the experimental spectra to arrive at a better agreement, here an alignment with respect to the VBM is preferred. To this end, a value

of 80.1 eV for the absolute energy of the Al $2p$ core level is estimated by adding the Fermi energy of Al to the measured Al $2p$ energy of a very thin oxide.[36] Then, by substracting the calculated photoelectric threshold energy from this estimated Al $2p$ energy, the VBM of XPS and Al $L_{2,3}$ spectra is located at 71.3 eV. Brytov and Romashchenko[8] aligned the O K spectrum with respect to the Al K spectrum to allow the difference between the binding energies of Al $2p$ and O $1s$. Also, the Al $L_{2,3}$ spectra was aligned in such a manner that the energy difference yielded the energy of Al $K\alpha_1, K\alpha_2$. Then they located the VBM by the point of intersection of a straight line extrapolating the short-wavelength edge of the O K spectrum and background. Following Kowalczyk et al.,[47] Olivier and Poirier[13] determined the VBM of XPS by linear extrapolation of the segment of maximum negative slope to the background. Interestingly, our, and these two schemes as well, arrive at the same energy within the uncertainty of 0.2—0.3 eV. Adding the calculated photoelectric threshold to the estimated VBM energies in the experimental spectra, we predict 80.1, 536.3, and 1567.1 eV for the binding energies of Al $2p$, O $1s$, and Al $1s$ core states, respectively. These values are in agreement with those estimated by Olivier and Poirier.[13] Aligning the calculated state densities and experimental x-ray emission[8] and XPS spectra,[11] we next draw vertical lines from each experimental feature, as shown in Fig. 4, and arrive at an interpretation of the spectrum. The O K spectrum is known to
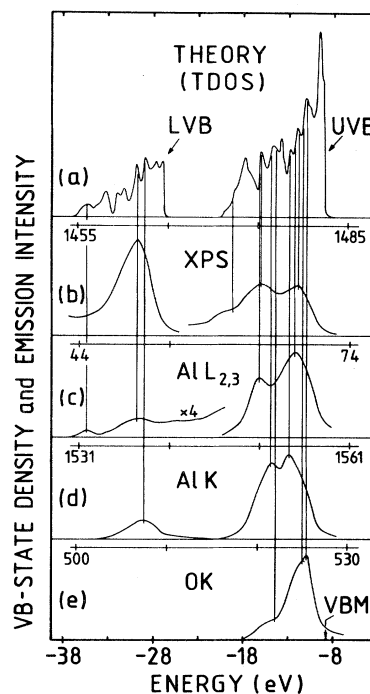

FIG. 4. Comparison of the valence-band density of states with various emission spectra. (a) Calculated total density of states of the valence band. (b) XPS spectrum reproduced from Ref. 11. X-ray emission spectra shown in panels (c), (d), and (e) are reproduced from Ref. 8. Energy scale pertaining to each spectrum is also given on the top of the corresponding panel.

sample mainly the O $2p$ valence states. In fact, the sharp peak at -11 eV coincides with the energy region of the calculated state densities where O $2p$ valence states have high density, and the shoulder at ~ -14.5 eV lies in the Al $3p$ —O $2p$ hybridization region. In accordance with the symmetry rules the bottom of the UVB, which is produced partly by the Al $3s$ orbitals, and the LVB, which is mainly O $2s$-like, are not sampled in the O K spectrum. Note that the O $2p$ orbital density of states (ODOS), with the exclusion of the steep peak near the VBM in Fig. 3(b), bears some resemblance to the O K curve. Our interpretation of Al K is based on the argument that valence states that have the Al $3p$ contribution are much more likely to participate in the transitions. The lower peak farther on the left of the spectrum may be associated with the LVB having a considerable Al $3p$ hybridization. Again, two features at the low binding energies at about -15 and -13 eV are produced by the Al $3p$ —O $2p$ hybridization states in the UVB. The Al $L_{2,3}$ spectrum samples more states of s-orbital symmetry, as clearly seen in the lower part of the spectrum. The lowest feature at about -35 eV is associated with the Al $3s$ —O $2s$ bonding states, and thus gives a clear indication about the width of the LVB. The feature at about -30 eV coincides with the dominant XPS peak, and is produced by the high-density O $2s$ states in the LVB. The Al$_{2,3}$ peak at -16.5 eV arises from the Al $3s$ —O $2p$ states in the UVB. The upper peak at ~ -12 eV exhibits highest intensity, and occurs at the upper part (i.e., O $2p$ band region) of the UVB. This situation is in contradiction with the arguments based on the symmetry of atomic orbitals, and may be attributed to the band-structure effects.[44] The XPS spectrum describes the valence band with an emphasis on s-like states. The dominant peak at the lower part of the spectrum is produced by the O $2s$ states of the LVB and thus confirms the above statement. Its asymmetric shape resembles the O $2s$ ODOS presented in Fig. 3(c). The upper region of the spectrum[11] seems to reproduce three broad features of the UVB. The shoulder at about -19 eV, which is not found in other spectra, seems to resolve the Al $3s$ —O $2p$ hybridization region.

As for the conduction band, the spectrum of interest is brought forth by the excitation of the valence or core states to the conduction band, to the excitons constructed therefrom, or to other empty states originating from the defects. The joint density of states enters through the transitions from the valence band to the the conduction band and hence makes it difficult to extract information concerning the CB alone from the corresponding spectrum. The initial states are dispersionless in the transitions from the core states, and consequently, of course to some extent, the intensities of O K, Al K, and Al $L_{2,3}$ spectra[8] reflect the density of the CB states. The difficulty in the x-ray absorption spectra arises from the low-energy structure associated with the excitons, or empty defect states. Locating the VBM in the emission spectra and thereby aligning the calculated state density with respect to them, we may easily mark the CB edge in the absorption spectra to coincide with the CBm of the calculated state density.[48] This way, we arrive at Fig. 5, which displays the state density of the CB, and the absorption spectra reproduced from Ref. 8 in the absolute energy scale. We did not perform a detailed analysis of the selec-
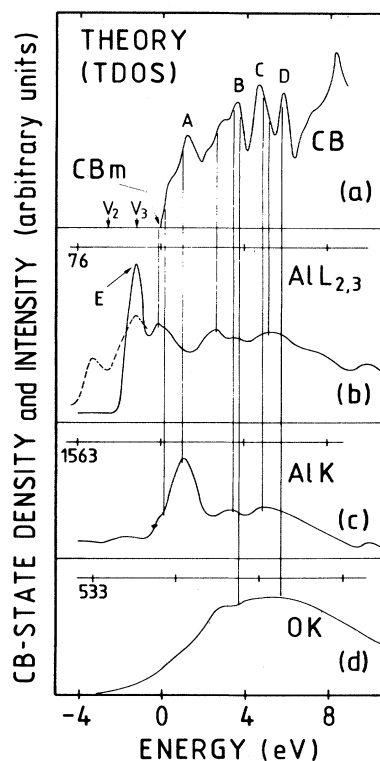

FIG. 5. Comparison of the conduction-band density of states with various excitation spectra reproduced from Ref. 8. Main features of the calculated state densities are labeled by A, B, C, and D. V_2 and V_3 in panel (a) indicate the calculated O-vacancy states near the edge of the conduction band. The excitation spectrum of amorphous Al$_2$O$_3$ is shown by the dashed lines in panel (b). The energy scale of each spectrum is presented on the top of panels.

tion rules. Thus the rest of our interpretation relies on the comparison of the observed features with the state density. The low-energy structure of the Al $L_{2,3}$ excitation spectrum lies in the band gap. Similar structures have been observed in the vacuum ultraviolet (vuv) optical[6] and soft x-ray absorption[7] spectra, and were interpreted to imply the exciton absorption. However, it should be borne in mind that this structure, or part of it, may be brought about by the defect states. Such a possibility will be discussed in the next section. In the calculated state density there are features, which are labeled by A, B, C, and D, which coincide with the various features of the experimental spectra. The peak A lies at about 1.5 eV, and is produced mainly by the flat band in the vicinity of the Y point in the BZ. The dominant peak of the Al K spectrum is attributed to the states of A. The broad feature B, extending from ~ 2 to 4 eV, is produced from the flat Al $3s$ —Al $3p$ bands. The shoulder at 3 eV coincides with the third peak in the Al $L_{2,3}$ spectrum, whereas the high-density peak at 4.6 eV corresponds to features of Al K and O K spectra. The features of Al $L_{2,3}$ and Al K spectra lie under the peak C at ~ 5 eV. The overall agreement with the excitation spectra and the calculated CB density of states is good, except for the intense peak of the Al $L_{2,3}$ spectrum lying just at the absorption edge. Certainly, the

lowest conduction band would contribute to the upper edge of this peak, but the high-density region should result from the final states having a different origin. We will turn to this point shortly.

Finally, the peak positions in the EELS spectrum[13] correspond to transition from the valence- to conduction-band states, and hence substantiate the above interpretation. Low-energy structures at 3.8, 4.2, and 5 eV bear upon the defect states. By examining the state densities in Fig. 3 we conclude that the EELS features at 12.6, 16.5, and 20.7 eV result from the transitions between the UVB and the CB states. The 12.6-eV peak is ascribed to the transition from the O $2p$ valence-band states to the empty states producing the peak A in the conduction band. The 16.5-eV transition can take place either from the high density of states ~ -16 eV to the peak A or from the O $2p$ valence-band states at ~ -11.5 eV (that give rise to the sharp peak of O K emission spectrum) to the peak C in the conduction band. Either, the high density of states at -16 eV (that gives rise to the features in the XPS and Al $L_{2,3}$ spectra), or the states at ~ -19 eV (that give rise to the low-lying XPS feature) can be an initial state of the 20.7-eV transition. For the former the peak C should be the final state, whereas the peak A is associated with transition from the latter initial state. Nevertheless, the selection rules should inhibit one of these transitions or mix both. The peak lying at the high-energy side of the EELS spectrum is associated with the LVB. The difference in energy between the high density of states of the LVB at ~ -29.5 eV and the peak A is very close to the 30.3-eV EELS transition, and thus confirms the previous interpretation.[13]

Before we terminate our discussion we comment also on the previous band models. In the interest of our readers, basic values of the electronic structure extracted from

various experimental and theoretical investigations are summarized in Table II. To provide a semiquantitative account of the band structure of α-Al$_2$O$_3$, Reilly[23] employed a linear combination of atomic orbitals—molecular orbitals (LCAO-MO) method and idealized the atomic configuration to result in O sp^2 and Al sp^3 directed bonds. His band model displays a 12 eV wide UVB with three separated regions and a 4 eV wide LVB. Douglas[24] used an $ad\ hoc$ crystal potential generated by superimposing the screened Coulomb potential and obtained a band model which has a considerably large UVB (~ 13 eV) and a 10 eV wide LVB. The dispersions of the bands are at variance with ours. In addition to these studies there are two recent calculations that deserve a detailed discussion. The first one is the semiempirical calculations of Evarestov $et\ al.$,[27] wherein the charge self-consistency was achieved using effective atomic charges defined by the Löwdin's canonical orthogonalization scheme[49] and four $\vec{k}$ vectors in the BZ. The second one was carried out by Batra[28] using a first-principles method with a crystalline potential generated from the overlapping atomic charge densities. The upper valence bands calculated by Evarestov $et\ al.$ are about 12 eV wide, whereas Batra obtains a width of about 6 eV. The lower valence bands (the O $2s$ region) are 5.4 eV wide in the former calculation, whereas Batra gives a value of about 3 eV. One very interesting feature at which both these calculations arrive is the intraband gap, i.e., $E(\text{UVBm}) - E(\text{LVBM})$, which is about 10 eV wide, whereas experimentally the value is $5-6$ eV. It appears that the first-principles calculation leads to bands that are considerably narrow as compared to the bands obtained from the semiempirical methods.[50] α-alumina is known to be a highly ionic solid and is normally expected to have narrow bands. Wide bands, especially the wide LVB are somewhat unexpected, but they seem to be confirmed by

TABLE II. Some important values (in eV) of the band structure of α-alumina: the energy gap, the photoelectric threshold, the width of the UVB, the gap between the UVB and the LVB, the width of the LVB, the width of the VB, and the separation between O $2s$ and the second dominant peak of the UVB. Corresponding references are indicated.

	Experiment	Present study	ETB[a]	MR[b]
E_g (Energy gap)	9.9,[c] 8.5[d]	8.7	~ 8.0	36.1
E (VBM)	-8.5[d]	-8.8		-9.0
$E(\text{UVBM}) - E(\text{UVBm})$	10.6,[e] 11[f]	11.8	6.0	12.1
	~ 15.0,[g] 11.6[h]			
$E(\text{UVBm}) - E(\text{LVBM})$	~ 6.0,[i] ~ 4.0[g]	6.3	10.0	10.4
$E(\text{LVBM}) - E(\text{LVBm})$	~ 9.0,[i] ~ 6.0[g]	9.5	3.0	5.4
$E(\text{UVBM}) - E(\text{LVBm})$	~ 28.0,[i] ~ 27.0[f]	27.6	18.6	28.2
	~ 26.0[h]			
$E_2 - E_4$	13.3,[e] 13.5[f]	13.8	~ 10.8	~ 16.7
	~ 13.5,[g] 13.6[h]			

[a]Reference 28 (extended tight-binding method).
[b]Reference 27 (Mulliken-Rudenberg method).
[c]Reference 6.
[d]Reference 13.
[e]Reference 9.
[f]Reference 10.
[g]Reference 11.
[h]Reference 12.
[i]Reference 8.

the experimental data presented in Table II. One possible explanation of this puzzling result can be found in Fig. 1(c). The more charge is transferred from Al, the higher becomes the hybridization between Al and O orbitals. As a result the UVB and the LVB become broader, and thus the intraband gap recedes. Stated differently, increasing ionicity is counterbalanced by the induced covalent component. For a perfect ionicity the values of the effective charges would be Al^{3+} and O^{2-}, which is roughly what Batra finds. Evarestov *et al.* find Al^{1+} and $O^{2/3-}$ as the final self-consistent configuration, which is close to the value obtained in the present study. At this point mention should be made that one has to be cautious when comparing the effective charges obtained from different methods of calculations. As a matter of fact there is no unambiguous definition of the effective charge. Even though LCAO-type approaches provide a simple concept for the definition of the effective charge, the calculated values depend upon the off-diagonal terms, and of course upon the form of the atomic orbitals. With this caution in mind one can argue that in Batra's calculation the overlap population is large because of the extended basis sets on Al and O, and because the lack of self-consistency provides too high an ionicity.

A serious shortcoming of the calculation of Evarestov *et al.* is that it arrives at a forbidden band gap of about 36 eV, and the experimental value is about 9 eV. In the semiempirical method the conduction-band states are unstable due to the fact that the antibonding combination of the overlap matrix amplifies the small changes in the Hamiltonian matrix elements. Nevertheless, both of these calculations have provided some fundamental understanding of the electronic structure of α-alumina and in the present work we clarify some of these points.

FIG. 6. Atomic arrangement of the ideal α-Al₂O₃(0001) surface. The surface unit cell is shown by the bold lines. Numbers in the circles denote the atomic layers. Oxygen atoms represented by black circles lie at the second layer, and the z axis is taken perpendicular to the surface.

empty and doubly degenerate because of the two slab surfaces. The states of these bands are produced by the $s + p_z$ dangling bonds of the surface Al atoms with a considerably small O orbital contribution from the second layer. The occurrence of the dangling bond can be visualized by examining the atomic arrangement shown in Fig. 6. The

IV. ELECTRONIC STRUCTURE OF DEFECTS

A. α-Al₂O₃(0001) surface

As a first attempt to study the electronic structure at room temperature we consider the ideal surface in the hexagonal axes. Figure 6 illustrates the atomic positions[17,18,51] and the surface unit cell. We simulate the surface by a slab having the thickness of the hexamolecular cell and a threefold rotation axis along z. The slab unit cell contains 12 Al and 18 O atoms in accord with the ideal bulk stoichiometry. Al atoms form the topmost surface layers on both sides of the slab. Each surface Al is connected to three O atoms of the second layer by a strong Al—O bond. Below the second layer the bond order between Al and O is bulklike. By iterating the effective charges of atoms at the surface region we carry out calculations consistently. During each iteration the effective charges are computed using 15 $\vec{k}$ points in the irreducible part of the surface BZ. The new orbital energies are obtained in Eq. (3) and are used as an input in the next iteration. Iteration cycles are continued until the differences between input and output charges are less than 0.1 electron. Figure 7 illustrates the calculated electronic energy structure. The most significant effect of the surface appears as the surface state bands S_d and S_p located in the gap. The flat band lying at ∼3 eV above the VBM is
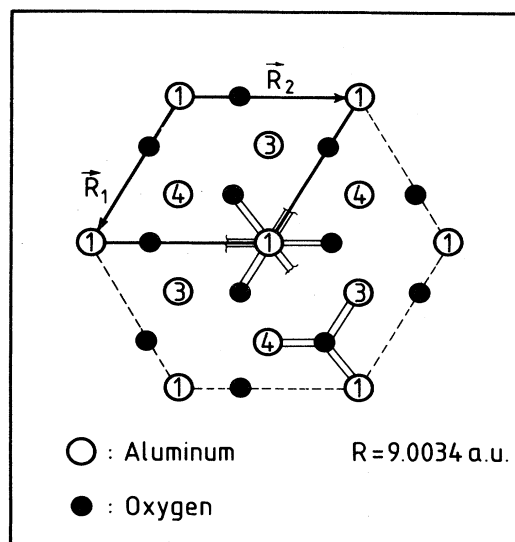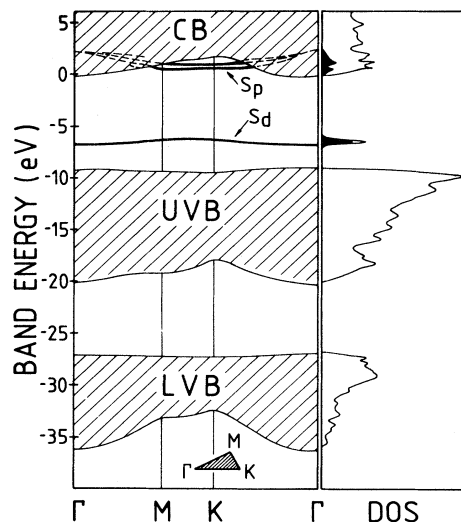

FIG. 7. (a) Energy-band structure of the ideal α-Al₂O₃(0001) surface represented by a 18-layer slab. S_d and S_p are the surface-state bands. The gaps in the VB and the CB are not shown. (b) The total density of states with the shaded area indicates the contribution of the surface Al atoms on the surface-state (S_d, S_p) densities.

oxygen atoms (forming an equilateral triangle at the second layer) are considered as the three corners of the tetrahedron and the position of the surface Al can be idealized to coincide with the center of this tetrahedron. Then, the surface Al is connected to these three oxygens and has one dangling bond directed to the empty corner. For the surface Al the consistent calculations lead to the effective charge which is smaller than that obtained by counting the bonds [i.e., $Q(\text{surface}) = Q(\text{bulk})/2$]. Al atoms at the third layer provide some excess charge to O atoms at the second layer, which in turn have effective charges comparable to that of the bulk. During the self-consistency cycles we observed that the location of S_d is strongly dependent on the effective charge of the surface Al atoms, and increasing charge depletion lowers the S_d band. Both the formation of the tetrahedral-like coordination at the surface and a charge transfer different from the bulk cause the Al—O bonds at the surface to become less ionic. As a result the oxidation state of the surface Al varies from that of the bulk. Furthermore, one may expect that the surface Al atoms rise from their ideal position still ensuring the (1×1) LEED pattern.[52] This certainly shifts the surface-state band located in the fundamental gap. At this point, we recall the observations of Norman et al.[22] made for the oxidation of the Al(111) surface. They suggested that the Al—O bonds above the surface (in which surface Al is surrounded by three surface oxygens) display a character different from those in the bulk. Surface states at the edges of the CB are derived from the conduction-band states and are produced mainly by Al $3p_{x,y}$ orbitals with some contribution from the second and third layers. In addition to these gap states we are able to locate surface resonances near the edges of the LVB and UVB. The total density of states in Fig. 7(b) exhibits a striking similarity to that of the bulk oxide, except for the structure in the gap and an enhancement near the CBm. The contribution of the surface Al shown by the dark area leads to the conclusion that the surface states are Al-like.

B. Vacancy states

To understand the electronic structure of vacancy, and more importantly the states originating from the bond orders differing from that of the bulk, we use a rather crude model. We simulate the ideal vacancy by a $(2 \times 2 \times 2)$ supercell, where one atom (Al or O) is removed at the defect site, but no lattice relaxation is taken into account. The supercell is used to ensure that defect-defect interaction is small, though a larger cell would be more desirable. Also the end effects inherent to the cluster-type calculations are avoided in the present model. To create an O vacancy one has to break four bonds, whereas the creation of an Al vacancy requires the breaking of six bonds. In that respect one can argue that the concentration of the anion vacancy is higher.

The supercell of the O vacancy contains 32 Al atoms and 47 O atoms. Although we are not able to perform self-consistent calculations for such a large system, we nevertheless attempted to get some idea of the effect of charge redistribution near the defect site. We carry out two different calculations by diagonalizing the secular matrix at the center of the supercell BZ. In the first one, we

assume that near the vacancy the orbital energies were unaltered. In the second calculation, we assume that less charge is transferred from the surrounding Al atoms. Then, the orbital energies of the surrounding Al atoms are computed by using Eq. (3) and their bond order. In both calculations, we obtained three vacancy states in the band gap, though one normally expects to have four. The last one is probably merged in the CB. States obtained by using the bulk orbital energies are located at -8.1, -2.7, and -1.3 eV. Charge redistribution on the surrounding Al atoms causes these states to move to lower binding energies and to appear at -7.8, -2.5, and -1.2 eV. The orbital analysis reveals that these vacancy states result mainly from the surrounding Al orbitals. The lowest state, however, has a considerable amount of contribution from the second-neighbor oxygens. The conclusion we draw from these calculations is that the O vacancy brings forth three empty states in the gap, one above the VBM, two below the CBm. The energy positions of these states would certainly depend upon the relaxation of the surrounding atoms, and upon the charge redistribution, as well. Interestingly, work by Mozzacurati and Signorelli[53] gives evidence on the empty states near the CBm. The O divacancy, and the voids in the bulk solid, are expected to initiate even more localized states in the gap.[54] In contrast to this, but similarly to what one previously found in SiO$_2$,[15] the Al vacancy does not lead to any localized state in the fundamental gap.

Having examined the defect states let us now turn to the excitation spectrum, and discuss the low-energy structures. The Al $L_{2,3}$ excitation spectra[8] of a-, γ-, and a-Al$_2$O$_3$ exhibit pronounced differences especially near the absorption edge. As clearly seen in Fig. 5(b), amorphous Al$_2$O$_3$ yields structures $\sim 3-4$ eV below the CBM and 2 eV below the E peak of a-Al$_2$O$_3$. A similar situation was observed in the extinction coefficients[6,11] of a- and a-Al$_2$O$_3$. Recently, Balzarotti et al.[55] reported the soft x-ray absorption spectrum of Al$_2$O$_3$ in three different structural forms. At the threshold they observed one single peak (at ~ 76.5 eV), two maxima (at 76.8 and 77.4 eV), and one single peak (at ~ 78.7 eV) for a-, γ-, and a-Al$_2$O$_3$, respectively. Furthermore, they suggested that the splitting in γ-Al$_2$O$_3$ spectrum cannot be attributed to the spin-orbit splitting of the Al $2p$ levels, but should be associated with the empty final states. Here, an important observation one can make is that the low-energy absorption features in a- and γ-Al$_2$O$_3$ shift to even lower energies, though all three structural forms have almost the same VB state densities. One should also recall that a- and γ-Al$_2$O$_3$ display a poor crystalline order, and have noticeable concentrations of vacancies and even voids.[54] Therefore, on the basis of the present calculations, as well as of the above observations, the absorption features ~ 3 eV below the CBm can be attributed to the O vacancy, or stated differently, to the O deficiency. The peak at 78.7 eV [denoted by E in Fig. 5(b)] is shown to be an excitonic state.[55] The occurrence of the excitonic states near the CBm of SiO$_2$ was also proposed.[44,56,57] It is interesting to note that one of the calculated O-vacancy states coincides with the E peak. In Fig. 7(b), the empty surface states at the CBm are seen to increase the state density, thereby suggesting that the high intensity of the Al $L_{2,3}$ spectrum at ~ 80 eV originates from these surface states. Such a possibility was previous-

ly proposed for SiO_2.[15]

In accordance with what one finds in SiO_2,[15,56,58] the lower-lying surface or the O-deficiency states are the final states of the low-energy transition in the EELS spectrum. Olivier and Poirier,[13] in confirmation of our theoretical results, assumed that these low-energy structures are connected with the desorption of oxygen under prolonged electron bombardment.

V. CONCLUSION

We would like to stress some important aspects of our study by way of conclusion:

(i) By a realistic incorporation of the effect of charge transfer in the method we were able to calculate the electronic structure of α-Al_2O_3 which provides a consistent interpretation of the spectra.

(ii) We showed that the valence states of Al_2O_3 are mainly oxygenlike and grouped in two energy regions. The charge transfer from Al to O enhances the hybridization at the lower parts of the UVB and the LVB. The conduction-band states are mainly Al-like and have minimum at the center of BZ. The fundamental gap is found to be indirect.

(iii) The surface-state bands of the ideal α-$Al_2O_3(0001)$ surface are produced mainly by the Al orbitals. The energy positions of these bands are strongly dependent upon Al-O distance and the effective charge of the surface aluminiums. The bonds, which connect the surface aluminiums to oxygens at the second layer, are found to have a considerable covalent character. It is expected that the spectrum of the Al $2p$ core region can yield valuable information regarding the bonding at the surface.

(iv) A low bond order arising from the oxygen deficiency gives rise to empty gap states. The low-energy transitions in the EELS spectrum are explained in terms of these defect states. Furthermore, part of the low-energy structures on the soft x-ray spectrum of γ- and a-Al_2O_3, and also the enhancement at the absorption edge of α-Al_2O_3, can be attributed to these defect states.

ACKNOWLEDGMENTS

*Permanent address: Department of Physics, Middle East Technical University, Ankara, Turkey.

[1]D. L. Griscom, J. Non-Cryst. Solids 24, 155 (1977).

[2]*Proceedings of the International Conference on the Physics of SiO$_2$ and Its Interfaces*, edited by S. T. Pantelides (Pergamon, New York, 1978).

[3]R. L. Kurtz and V. E. Henrich, Phys. Rev. B 26, 6682 (1982).

[4]V. A. Fomichev, Fiz. Tverd. Tela (Leningrad) 8, 2892 (1966) [Sov. Phys.—Solid State 8, 2312 (1967)].

[5]K. Codling and R. P. Madden, Phys. Rev. 167, 587 (1968).

[6]E. T. Arakawa and M. W. Williams, J. Phys. Chem. Solids 29, 735 (1968).

[7]A. Balzarotti, A. Bianconi, E. Burattini, M. Grandolfo, R. Habel, and M. Piacentini, Phys. Status Solidi 63, 77 (1974).

[8]I. A. Brytov and Yu. N. Romashchenko, Fiz. Tverd. Tela (Leningrad) 20, 664 (1978) [Sov. Phys.—Solid State 20, 384 (1978)].

[9]C. G. Dodd and G. L. Glen, J. Appl. Phys. 39, 5377 (1968); J. Am. Ceramic Soc. 53, 322 (1970).

[10]D. W. Fischer, Adv. X-ray Anal. 13, 159 (1970).

[11]A. Balzarotti and A. Bianconi, Phys. Status Solidi B 76, 689 (1976).

[12]S. P. Kowalczyk, F. R. McFeely, L. Ley, V. T. Gritsyna, and D. A. Shirley, Solid State Commun. 23, 161 (1977).

[13]J. Olivier and R. Poirier, Surf. Sci. 105, 347 (1981).

[14]Much experimental work related to the defect states in SiO$_2$ can be found in *Insulating Films on Semiconductors*, edited by G. G. Roberts and M. J. Morant (IOP, Bristol, 1979).

[15]S. Ciraci and Ş. Erkoç, Solid State Commun. 40, 587 (1981); R. B. Laughlin, J. D. Joannopoulos, and D. J. Chadi, Phys. Rev. B 21, 5733 (1980); F. Herman and R. V. Kasowski, J. Vac. Sci. Technol. 19, 395 (1981); S. Ciraci and Ş. Ellialtioğlu, Phys. Rev. B 25, 4019 (1982), and references therein.

[16]J. M. Charing, Appl. Phys. Lett. 10, 139 (1967).

[17]C. C. Chang, J. App. Phys. 39, 5570 (1968).

[18]T. M. French and G. A. Somorjai, J. Phys. Chem. 74, 2489 (1970).

[19]An extensive review of the problems related to the oxidation of the Al surface was recently given by I. P. Batra, Top. Current Phys. 29, 55 (1982).

[20]S. A. Flodström, C. W. B. Martinson, R. Z. Bachrach, S. B. M. Hagström, and R. S. Bauer, Phys. Rev. Lett. 40, 907 (1978).

[21]P. Hofmann, C. V. Muschwitz, K. Horn, K. Jacobi, A. M. Bradshaw, K. Kambe, and M. Scheffler, Surf. Sci. 89, 327 (1979).

[22]D. Norman, S. Brennan, R. Jaeger, and J. Ströhr, Surf. Sci. 105, L297 (1981).

[23]M. H. Reilly, J. Phys. Chem. Solids 31, 1041 (1970).

[24]F. C. Douglas, Ph.D. thesis, University of Connecticut, 1970 (unpublished).

[25]J. A. Tossel, J. Am. Chem. Soc. 97, 4840 (1975); J. Phys. Chem. Solids 36, 1273 (1975).

[26]K. L. Brower, J. Vac. Sci. Technol. 12, 458 (1975).

[27]R. A. Evarestov, A. N. Ermoshkin, and V. A. Lovchikov, Phys. Status Solidi B 99, 387 (1980).

[28]I. P. Batra, J. Phys. C 15, 5399 (1982).

[29]R. Hoffmann, J. Chem. Phys. 39, 1397 (1963). For a recent discussion of the method, see also D. W. Bullet, in *Solid State Physics* edited by H. Ehrenreich, F. Seitz, and D. Turnbull (Academic, New York, 1980), Vol. 35.

[30]P. G. Perkins, D. R. Armstrong, and A. Breeze, J. Phys. C 8, 3558 (1975); O. Bisi and C. Calandra, *ibid.* 14, 5479 (1981).

[31]I. P. Batra and O. Bisi, Surf. Sci. 123, 283 (1982).

[32]J. C. Slater, Phys. Rev. 36, 57 (1930).

[33]E. Clementi and D. L. Raimondi, J. Chem. Phys. 38, 2686 (1963).

[34]M. Nishida, J. Chem. Phys. 63, 956 (1978); Surf. Sci. 109, 557 (1981).

[35]R. S. Mulliken, J. Chem. Phys. 23, 1833 (1955).

[36]H. P. Bonzel and H. J. Krebs (private communication).

[37]E. R. Il'mas and A. I. Kuznetsov, Fiz. Tverd. Tela (Leningrad) 14, 1464 (1972) [Sov. Phys.—Solid State 14, 1255 (1972)].

[38]M. L. Cohen and V. Heine, in *Solid State Physics* edited by H. Ehrenreich, F. Seitz, and D. Turnbull (Academic, New York, 1970), Vol 24; P. W. Anderson, Phys. Rev. 181, 25 (1969).

[39]R. W. G. Wyckoff, *Crystal Structures II,* 2nd ed. (Wiley, New York, 1964). For an elucidative discussion of atomic configuration and the symmetry properties of corundum structure one may refer to Refs. 27 and 28.

[40]S. Ciraci and I. P. Batra, Phys. Rev. B 15, 4923 (1977).

[41]By definition, the structural unit here differs from the Al_2O_3 molecular unit, and is deduced in consideration of the nearest neighbors. For example, the SiO_4 tetrahedron is taken as such a fundamental structural unit of β-crystobalite.

[42]T. H. DiStefano and D. E. Eastman, Solid State Commun. 9, 2259 (1971); Phys. Rev. Lett. 25, 1560 (1971).

[43]P. M. Schneider and W. B. Fowler, Phys. Rev. Lett. 36, 425 (1976).

[44]S. T. Pantelides and W. A. Harrison, Phys. Rev. B 12, 2667 (1976).

[45]J. R. Chelikowsky and M. Schlüter, Phys. Rev. B 15, 4020 (1977).

[46]I. P. Batra, in Ref. 2, p. 65.

[47]S. P. Kowalczyk, F. R. McFeely, L. Ley, R. A. Polak, and D. A. Shirley, Phys. Rev. B 9, 3573 (1974).

[48]S. T. Pantelides, Phys. Rev. B 11, 2391 (1975).

[49]P.-O. Löwdin, J. Chem. Phys. 18, 365 (1950).

[50]Although the widths of the bands are used as input values of our optimization, Fig. 1 designates that the calculated width of the LVB is already $\sim$7 eV prior to any change of the orbital energies.

[51]J. C. Slater, *Quantum Theory of Molecules and Solids II,* (McGraw-Hill, New York, 1965).

[52]The theoretical work by D. M. Bylander, L. Kleinman, and K. Mednick, Phys. Rev. Lett. 48, 1544 (1982), showed that the $2p$ core-level energy of the surface Al atoms exhibits a strong dependence on the distance of the O atom chemisorbed on the Al(111) surface. In view of the present results one may argue that the covalent component of the Al—O bond varies depending on the bond order and the bond length.

[53]V. Mazacuratti and G. Signorelli, Lett. Nuovo Cimento 12, 347 (1975).

[54]E. J. W. Verwey, J. Chem. Phys. 3, 592 (1975).

[55]A. Balzarotti, F. Antonangeli, R. Girlanda, and G. Martino, Solid State Commun. 44, 275 (1982).

[56]H. Ibach and J. E. Rowe, Phys. Rev. B 10, 710 (1974).

[57]R. B. Laughlin, Phys. Rev. B 22, 3021 (1980).

[58]V. M. Bermudez and V. H. Ritz, Phys. Rev. B 20, 3446 (1979).